AGU PUBLICATIONS

Geophysical Research Letters

RESEARCH LETTER
10.1002/2016GL068426

Key Points:
- Gravity and deformation signatures of the 26 October 2013 Mount Etna lava fountain
- Integrated finite element-based inversion of gravity and GPS data
- Inference on a highly compressible volatile-rich magma in the magmatic reservoir

Supporting Information:
- Supporting Information S1

Correspondence to:
F. Greco,
filippo.greco@ingv.it

Citation:
Greco, F., G. Currenti, M. Palano, A. Pepe, and S. Pepe (2016), Evidence of a shallow persistent magmatic reservoir from joint inversion of gravity and ground deformation data: The 25–26 October 2013 Etna lava fountaining event, *Geophys. Res. Lett.*, *43*, doi:10.1002/2016GL068426.

Received 26 FEB 2016
Accepted 22 MAR 2016
Accepted article online 28 MAR 2016

Evidence of a shallow persistent magmatic reservoir from joint inversion of gravity and ground deformation data: The 25–26 October 2013 Etna lava fountaining event

Filippo Greco[1], Gilda Currenti[1], Mimmo Palano[1], Antonio Pepe[2], and Susi Pepe[2]

[1]Istituto Nazionale di Geofisica e Vulcanologia, Sezione di Catania - Osservatorio Etneo, Catania, Italy, [2]Istituto per il Rilevamento Elettromagnetico dell'Ambiente, CNR, Napoli, Italy

Abstract To evaluate the volcanic processes leading to the 25–26 October 2013 lava fountain at Mount Etna, we jointly investigated gravity, GPS, and DInSAR measurements covering the late-June to early-November time interval. We used finite element modeling to infer a shallow magmatic reservoir which (i) inflated since July 2013, (ii) fed the volcanic activity at the summit craters during 25–26 October, and (iii) deflated due to magma drainage related to this volcanic activity. We suggested that this reservoir belongs to a shallow volume, which is located beneath the summit area and is replenished by magma rising from deep reservoirs and fed the short-term volcanic activity, representing a persistent shallow magmatic plumbing system of Etna. In addition, the model results show that there is a large discrepancy between the erupted and shallow reservoir deflation volumes, which could be reasonably attributable to a highly compressible volatile-rich magma.

1. Introduction

Over recent years, volcanic activity at Mount Etna has been characterized by the occurrence of violent lava fountaining episodes. In particular, between January 2011 and January 2014, 47 short-duration lava fountain episodes took place at the New South-East Crater (hereinafter NSEC; see inset in Figure 1) [*Calvari et al*., 2011; *Bonaccorso and Calvari*, 2013; *Behncke et al*., 2014]. Of these, 18 occurred between 11 January 2011 and 15 November 2011 [*Ganci et al*., 2012; *Bonaccorso et al*., 2013], 7 between 4 January 2012 and 24 April 2012 [*Behncke et al*., 2014], 13 from 19 February 2013 to 27 April 2013, and 9 from 26 October 2013 to 21 January 2014 [*De Beni et al*., 2015]. The time interval between any pair of lava fountaining cycles was characterized by a general absence of volcanic activity with the exception of mild and pulsating strombolian explosions and lava flows that occurred at the Bocca Nuova Crater (BNC; see inset in Figure 1) before the cycle started on 19 February 2013 [*De Beni et al*., 2015].

Such a continuous and prolonged explosive activity, accompanied by intense ash emission, has produced varying degrees of adversity in the Etnean towns. Therefore, the need to understand, recognize, and predict this explosive activity at Mount Etna is becoming of considerable importance and of great relevance for civil defense purposes. With this aim, a number of studies have focused on these events in order to unravel the processes leading to the explosive lava fountains [*Calvari et al*., 2011], to derive strict constraints on their timing of occurrence [*Bonaccorso et al*., 2011a, 2011b], and to estimate erupted volumes [*Ganci et al*., 2012].

Here taking advantage from the availability of time-lapse gravity measurements encompassing the 25–26 October lava fountain and coupling these measurements with those coming from the continuous GPS network, we present for the first time an integrated finite element-based inversion of the gravity variations and ground displacements related to the event. To properly evaluate the internal volcanic processes preparatory to the event, we took into account also gravimetric measurements carried out in July and October 2013 as well as continuous GPS and differential interferometry synthetic aperture radar (DInSAR) data covering the same period. Despite the difficulties in interpreting jointly these data, their complementarity enables for a valuable constraint on the subsurface magma movements [*Battaglia et al*., 2008]. Such an integrated study allowed us to infer a shallow magmatic reservoir that inflated since July 2013 and deflated while feeding the 25–26 October lava fountain as a consequence of the magma drainage.

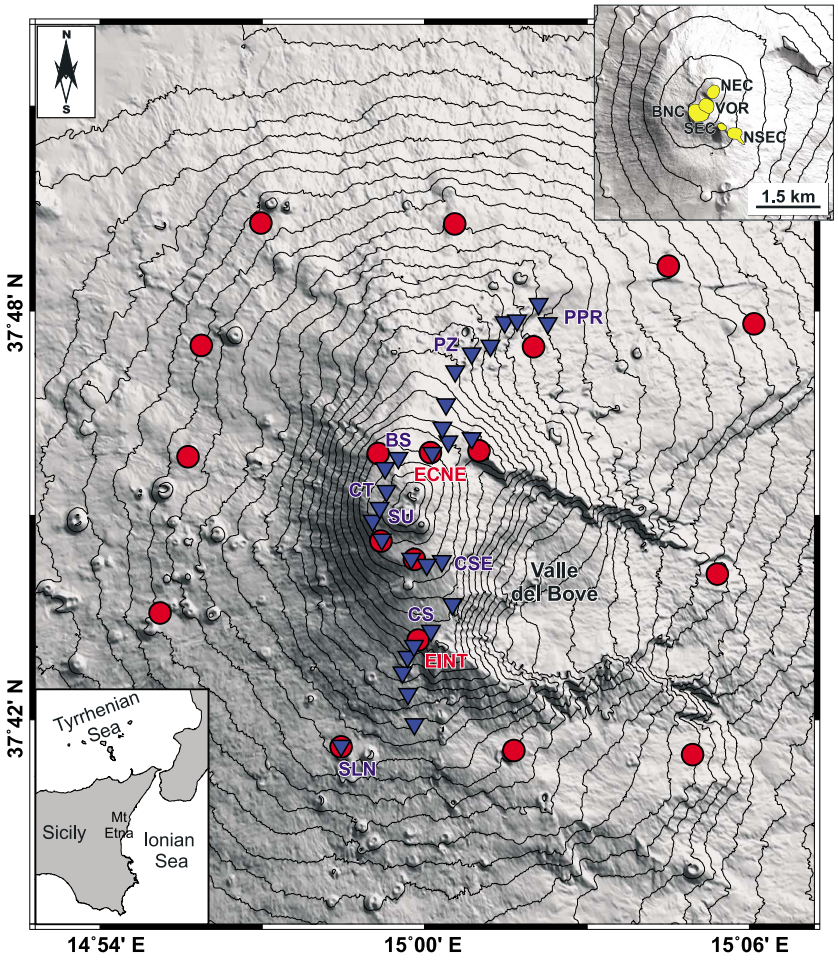

Figure 1. Map of Mount Etna volcano showing the location of the gravimetric (blue triangle) and GPS (red circles) stations used in this study. The top right inset shows the summit craters (NSEC, New South-East Crater; SEC, South-East Crater; NEC, North-East Crater; BNC, Bocca Nuova Crater; VOR, Voragine). The bottom left inset reports the geographical location of Mount Etna.

2. The 25–26 October 2013 Paroxysmal Event

After a pause of 6 months, the 25–26 October lava fountain episode marked the resumption of a new eruptive sequence, resulting in a total of nine events through late January 2014. The event was characterized by a lava fountain at the NSEC accompanied by the occurrence of a second ash plume at the North-East Crater (NEC) and the intracrater activity at the BNC. The episode started with explosive activity at the NSEC resuming at ~12:44 (all times are referred to the Greenwich Mean Time) on 25 October, gradually increasing in intensity and becoming a low lava fountain at ~01:30 on 26 October. Later, between 03:30 and 04:00, the lava fountain increased significantly in intensity, growing to about 500 m height and forming a significant ash plume, at which time explosive activity also started at the BNC. At 03:16 a lava flow started to pour out from the western rim of the NSEC [*De Beni and Behncke*, 2013]. At 06:21 also the NEC started erupting, with explosions and a pulsating plume of hot ash of grayish-brown color that lasted for ~1.5 h, while the lava fountain from the NSEC was still ongoing and a lava flow was spreading from the South rim of NSEC. Such a lava flow surrounded the crater to the SW, south, and then moved to SE, emerging at ~06:00 on the West rim of the Valle del Bove [*De Beni et al*., 2015]. Finally, the BNC produced sporadic explosions, one of which led to heavy fallout of lithic material (ash and blocks composed of old, mostly altered rock) onto the flank of the crater, forming a ground-hugging cloud resembling a pyroclastic flow. At NSEC, lava fountaining continued with slightly fluctuating intensity until about 10:00, and subsequently, the intensity decreased rapidly until ~13:00. A total volume ranging within the $1.1–2.1 \times 10^6\ m^3$ interval was erupted during the event, as estimated by the areal extension and thickness of the erupted lava field [*De Beni et al*., 2015].

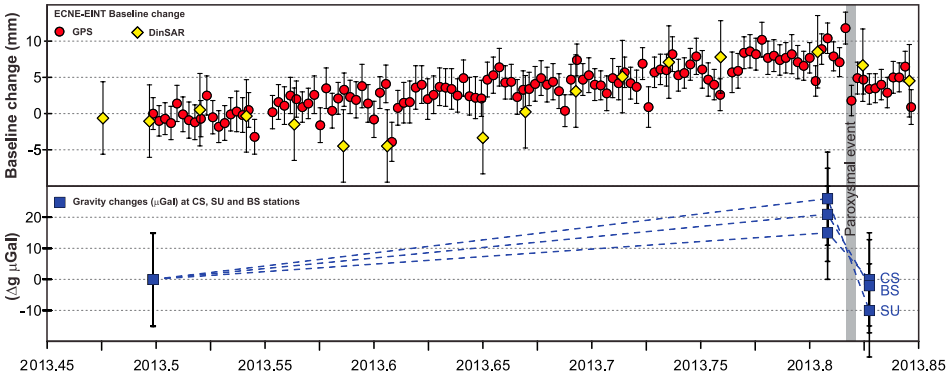

Figure 2. (top) GPS-based and time series of ECNE-EINT baseline; DInSAR time series between two pixels close to ECNE and EINT GPS stations. (bottom) gravity changes at some selected stations located to the summit area.

3. Data

3.1. GPS Observations

The Mount Etna continuous GPS network began to operate in late 2000. The network geometry was upgraded over time to reach the current configuration of 39 stations that densely cover most areas of the volcano edifice (Figure 1). To study the ground deformation pattern related to the 25–26 October 2013 lava fountain episode, as well as to cover the same interval sampled by microgravity measurements, we analyzed continuous GPS data collected between 1 July 2013 and 5 November 2013. GPS data were processed using the GAMIT/GLOBK software [*Herring et al.*, 2010] following the strategy described in *González and Palano* [2014].

To detect significant signals related to Mount Etna activity, we analyzed the daily baseline changes for ECNE and EINT stations because they were continuously operating throughout the investigation period (Figure 2). In addition, since both stations are located close to the summit area and their baseline crosses the crater area in a ~N-S direction, this baseline is able to track the movement of magma within the shallower portion of Mount Etna's plumbing system. This baseline allowed us to detect two time intervals characterized by (i) a lengthening of ~1.3 cm from the beginning of July to 25 October and (ii) a shortening of ~1 cm in response to the 25–26 October 2013 lava fountain episode. Therefore, we computed the ground displacement fields for the 1 July to 25 October 2013 (hereinafter I1) and 25–26 October 2013 (hereinafter I2) periods. The former spans a period similar to the one covered by gravimetric measurements (1 July to 22 October 2013), while the latter samples the lava fountain episode. During interval I1, the ground deformation field is characterized by a radial pattern in the horizontal displacements (Figure 3a), suggesting an inflation of the volcano. Although characterized by positive values, the observed vertical variations during I1 are not particularly relevant because the observed changes are within the associated uncertainties (Figure 3b). During interval I2, the ground deformation field reversed, clearly indicating a slight deflation of the summit area (Figures 3d and 3e).

3.2. DInSAR Analysis

To obtain an overall picture of the deformations occurring at Mount Etna, we also performed a DInSAR investigation by processing a set of 146 ascending SAR images acquired by the Cosmo-SkyMed constellation sensors (see supporting information) from 12 July 2009 to 10 January 2015. From this extensive data set, a group of 309 DInSAR images have been generated, which were inverted through the Small Baseline Subset (SBAS) technique [*Berardino et al.*, 2002] to retrieve the radar line-of-sight (LOS) displacement time series of the area over a set of coherent pixels [*Pepe and Lanari*, 2006]. Then, we extracted the deformation time series spanning the 21 June 2013 to 4 November 2013 time interval (Appendix A and Figure S1 in the supporting information). The SBAS processing chain includes operations for high-performance space-time phase unwrapping [*Pepe and Lanari*, 2006; *Yang et al.*, 2013] and the estimation and removal of residual phase artifacts (e.g., orbital, topographic and atmospheric artifacts/disturbances). As a final result, we derived the (geocoded) cumulative displacement maps (with a 30×30 m spatial resolution) for the two consecutive time intervals, which cover periods similar to those covered by gravimetric and GPS measurements: from 21 June to 19 October 2013 and from 19 October to 4 November 2013, respectively (Appendix A and Figure S1 in the

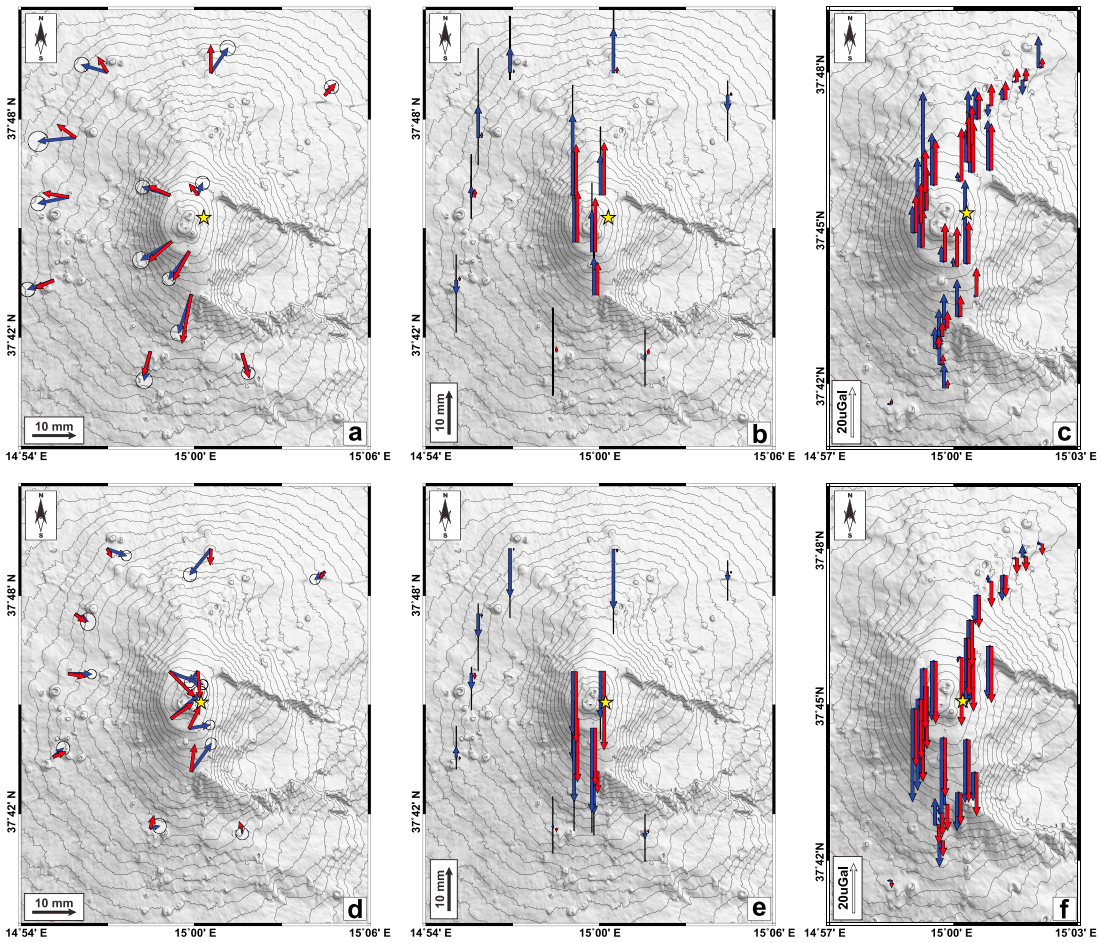

Figure 3. Blue arrows stand for measured (a and d) horizontal, (b and e) vertical GPS displacements, and (c and f) gravity variations for interval I1 and I2, respectively. Displacement uncertainties are at the 95% level of confidence. Expected displacements and gravity variations for I1 and I2 are reported as red arrows. Surface projection of modeled sources is reported as yellow stars (see Table S1 in the supporting information).

supporting information). It is also worth noting that available SAR acquisitions covering the two analyzed periods are quite limited in number, thus making difficult the retrieval of the two inherent DInSAR mean velocity maps. Accordingly, we focused on the two cumulative displacement maps (Figure S1), which, however, might be more influenced by the presence of noise and/or partially uncompensated atmospheric artifacts.

To evaluate the overall goodness of the achieved DInSAR results and therefore establish if the ongoing deformation signals lie within the accuracy of the DInSAR measurements, we compared the DInSAR deformation time series to available GPS measurements. To this aim, GPS data were projected along the radar LOS in order to make SAR and GPS measurements mutually comparable (Figure S1 in the supporting information). The standard deviation of the difference between SAR and GPS time series is (Figures S1c–S1h) of ~2 mm in correspondence to the GPS stations located in the upper western flank (e.g., EMEG and EMAL) and of ~6 mm in correspondence to the GPS stations located in the summit area (e.g., ECNE and EINT). These values are in general agreement with those estimated from previous SBAS time series quantitative analyses [*Casu et al*., 2006], resulting into an average accuracy of ~5 mm.

The 21 June to 19 October 2013 DInSAR LOS cumulative displacement map (Figure S1a) shows that the western flank of the volcano, as a whole, was approaching the sensor, whereas the summit area was moving away from the sensor and was characterized by weak deformation signals that, unfortunately, are barely detectable from SAR (being its values less than SBAS accuracy). Moreover, the DInSAR LOS cumulative map related to the 19 October to 4 November 2013 period shows that the western flank undergoes few millimeters motion away from the sensor (Figure S1b). We finally remark that although the DInSAR-based displacement maps provide an overall picture of the volcano ground deformation in agreement with the ones

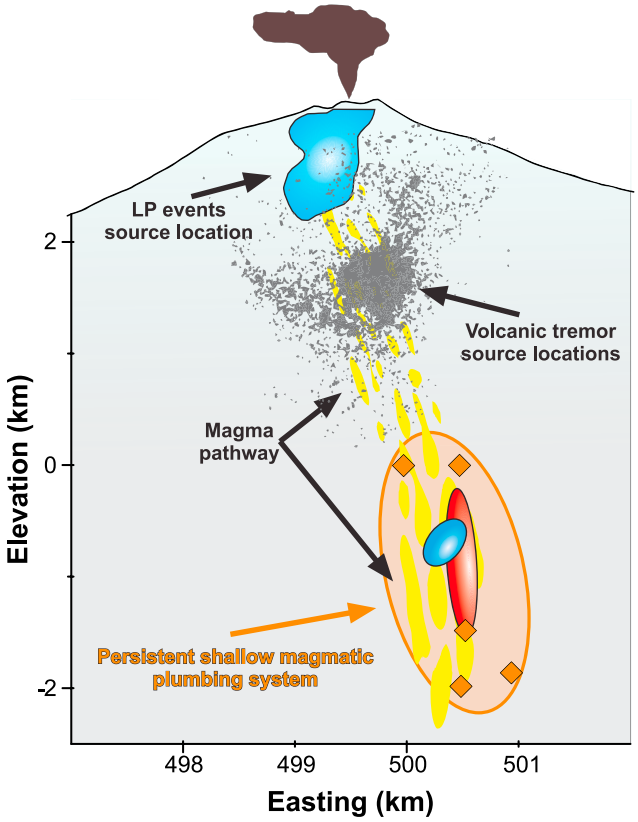

Figure 4. Schematic W-E vertical section crossing the summit area of Mount Etna showing the modeled sources (red and blue ellipses for I1 and I2 periods; see Table S1). LP and tremor source locations [*Cannata et al.*, 2015], as well as the inflating/deflating sources (orange diamonds) inferred since 2001 [*González and Palano*, 2014; *Patanè et al.*, 2013; *Bonaccorso et al.*, 2013], are also reported.

depicted by GPS data, however, the retrieved amplitude signals are at most on the order of SBAS accuracy. Therefore, we discarded them for the following analyses.

3.3. Microgravity Observations

Microgravity data were collected along the Summit Profile, which runs from Serra La Nave (SLN; 1740 m above sea level (asl)) in the southern flank to Piano Provenzana (PPR; 1800 m asl) in the northern flank, across the summit area of the volcano (3000 m asl; Figure 1). The profile includes 29 benchmarks located within 1 km from each other and close to, or coincident, with GPS stations (Figure 1). Quasi-monthly measurements are executed along this profile only during summer time; however, in order to follow the evolution of particular events, additional measurements are also carried out.

Gravimetric measurements were arranged by adopting the "profile method": the benchmarks are occupied in sequence, and the profile is traversed at least 2 times. The relative gravimeters Scintrex CG-3M#9310234 and CG5#300630040, periodically calibrated through the CTA-SLN absolute calibration line [*Greco et al.*, 2012], were used during the surveys. Data were adjusted for tidal effects using a local tide model, corrected for the instrumental drift, and referred to the SLN absolute station (Figure 1) [*Greco et al.*, 2012, 2015]. For each survey, an average error ranging in the ±10 to ±15 μGal interval is attained [*Pistorio et al.*, 2011]. Thus, at the 95% level of confidence, the uncertainty on temporal gravity differences is between ±14 and ±21 μGal.

Here we report the measurements (three surveys) carried out during a period lasting about four months (1 July to 29 October 2013) which encompass the 25–26 October 2013 lava fountain episode (Figure 2). Since the GPS measurements covering the same time intervals show small height variations (~4–8 mm) on stations placed close to the gravity benchmarks (Figures 4b and 4f), the free-air effect is within 1–2 μGal on the basis of the free-air gravity gradients measured in the summit area of Mount Etna [*Greco et al.*, 2012; *Maucourant et al.*, 2014]. Because the free-air effect is negligible if compared to the observed gravity changes and their associated uncertainties, we do not correct for such an effect.

Figure 2 shows the temporal gravity variations at the stations CS, BS, and SU (Figure 1), referred to the 1 July survey. The gravimetric measurements show a gravity increase with an amplitude of ~30 μGal at the station SU during the 1 July to 22 October 2013 period, and a marked −40 μGal gravity decrease at the same station during the 22–29 October 2013 period that encompassed the 25–26 October paroxysmal event.

The gravity variations observed at all stations of the profile between 1 July and 22 October 2013 (I1) exhibited a common positive pattern at the scale of the profile, mostly within 20 μGal, and only in two stations (CSE and CT) reached values of ~40 μGal (Figure 3c). Northward, the amplitude of the gravity change decreases rapidly, being almost within error at benchmarks PZ (Figure 3c).

The gravity variations observed at all stations of the profile during the 22–29 October 2013 period showed a decrease reaching −40 μGal, with a wavelength of about 6 km, centered on the stations in the summit area (Figure 3f).

4. Data Modeling

Deformation and gravity changes are jointly modeled using the finite element (FE) method, which has been recently used for interpreting deformation and gravity fields in volcanic areas [*Currenti et al*., 2007, 2008; *Trasatti and Bonafede,* 2008; *Currenti*, 2014]. The FE deformation and gravity solutions are embedded in a Genetic Algorithm inversion procedure [*Currenti et al*., 2008; *Carbone et al*., 2007] where the source parameters (position, geometry, volume change, and density variations) iteratively converge toward the best solution, which minimizes the misfit between the computed FE solutions and the observed geophysical changes.

As above mentioned, since DInSAR-based deformation maps might be affected by noise and/or partially uncompensated atmospheric artifacts and display a poor LOS accuracy (~5 mm), they are not suitable enough to perform a joint inversion; therefore, only GPS and gravity data are exploited for the following analyses. The 3-D FE model is set up to jointly compute deformation and gravity changes by solving the elastostatic and gravity problems for a finite spheroidal pressure source accompanied by interior density changes. The use of this numerical approach provides the opportunity to explore different magma chamber geometry and allows for medium heterogeneities and volcano topography, all factors that cannot be taken into account using standard analytical models. Two inversions were performed for the deformation patterns and gravity changes recorded before (I1) and during (I2) the lava fountaining event. The inverted source parameters, as well as a detailed description of the model setup, are reported in the supporting information.

Since the modeled sources are not spherical, there are nonzero deformation effects on gravity changes resulting from volumetric strain and from displacement of preexisting density gradients [*Currenti*, 2014]. The numerical estimates of these contributions to gravity changes are within ±3 μGal and, hence, could be neglected (see supporting information). The best solution inferred for I1 is given by a vertically elongated inflating source located beneath the eastern side of the summit area at 0.8 km below sea level and characterized by a volume change of 1.4×10^6 m^3 (see Table S1 in the supporting information). The best solution inferred for I2 indicates a deflating source, which is slightly elongated horizontally and located close to the source inferred for I1 (Table S1). For both time intervals, the goodness of fit between observed and modeled data is provided by the root-mean-squared error statistical parameter (Table S1).

5. Discussion and Conclusions

This study exploits an exceptional set of gravity measurements performed along the Summit Profile carried out 3 days before the 25–26 October lava fountain and immediately repeated a few days after the event. In addition, since this event also produced detectable ground deformation (less than 1 cm of horizontal displacement) of the upper sector of the volcano, we took into account all the available geodetic data. Moreover, to infer magma accumulation within the magmatic reservoir feeding the lava fountain (and likely the entire October 2013 to January 2014 cycle), we also analyzed available gravimetric, GPS and DInSAR measurements since June 2013.

We are aware that gravimetric and geodetic signals associated with the investigated periods are only slightly higher than their associated accuracy; however, their consistent overall patterns provide insight into subsurface magma movements. Despite the limitation due to the low signal/noise ratio, our finding represents a valuable example of multidisciplinary approach at the forefront of combining GPS and gravity measurements in a 3-D numerical inversion. Indeed, the FE-based joint inversion of both gravimetric and GPS measurements, allowed us to identify the sources acting before and during the 25–26 October lava fountain. They are located beneath the eastern side of Mount Etna summit area at shallow depth. Based on the position and associated uncertainties the inferred sources are probably attributable to a single source or at least could represent adjacent portions of a unique shallow magmatic reservoir (Figure S4). Such a shallow magmatic reservoir pressurized since July 2013 and fed the volcanic activity at the summit craters during 25–26 October. Hence, it depressurized (emptied) because of the magma drainage related to this volcanic activity.

This reservoir is located below the sources of the volcanic tremor and the LP events (Figure 4), which for the period analyzed here have been located at a depth >1 km asl and >2 km asl, respectively [*Cannata et al*., 2015].

In addition, it spatially overlaps a shallow volume where the presence of inflating/deflating sources has been detected at least since 2001 [*González and Palano*, 2014; *Patanè et al*., 2013; *Bonaccorso et al*., 2013]. Moreover, this shallow volume matches well with the magma ponding zones inferred by petrochemical analysis on magmatic rocks erupted during lava fountains that occurred in the last two decades [e.g., *Corsaro et al*., 2013]. These observations suggest that this volume represents a persistent shallow magmatic plumbing system of Mount Etna: this magmatic reservoir is supplied and probably replenished with magma rising from deep reservoirs that feed the short-term volcanic activity (e.g., strombolian and fountaining events). Indeed, clear evidence of a gradual pressurization of the deep portions of the plumbing system, started in late April 2013, is confirmed by tilt, GPS ground deformation, and CO_2 flux [*Cannata et al*., 2015].

The joint analysis and modeling of deformation and gravity measurements permits estimation of the volume changes of the magmatic reservoir before and during the eruptive event. The source underwent a volume increase of $0.9 \times 10^6\,m^3$ during I1 and a volume decrease of $-0.5 \times 10^6\,m^3$ during I2. The latter is less than the volume erupted during the lava fountain ($1.1–2.1 \times 10^6\,m^3$) [*De Beni et al*., 2015]. Two possible explanations can be suggested to properly account for the discrepancy between the erupted volume and the shallow reservoir deflation volume. As a first explanation, fresh magma could have refilled the reservoir during the lava fountaining episode in response to the drop in pressure in the reservoir; such a drop creates a pressure imbalance with a deeper magma source, promoting a fast ascent of fresh magma from the deep source into the reservoir. Alternatively, the observed discrepancy can be attributed to magma compressibility that may accommodate an additional batch of magma [*Palano et al*., 2012; *Kozono et al*., 2013; *Bonaccorso et al*., 2013; *Currenti*, 2014].

Regarding the first explanation, preliminary petrochemical analyses carried out on the products erupted during the 25–26 October lava fountain as well as on those erupted in the successive lava fountaining events provided evidence of fresh magma only after late November 2013 [*Corsaro and Miraglia*, 2013]. This aspect lends credence to a gradual refilling of the shallow reservoir instead of a fast ascent of deep magma. However, such continuous refilling must have occurred at a low rate since it was unable to balance the budget of emitted magma during the whole October 2013 to January 2014 lava fountaining cycles as indicated by the volcano-scale deflation that started in late October 2013 [*Cannata et al*., 2015].

Regarding the second explanation, during the main recharging phase, the ratio between gravity and height variations is indicative of an overall mass increase within the volcano with limited ground deformation, suggesting poor correlation between the reservoir volume and the arrival of fresh magma. This suggests that the magma was highly compressible and rich in volatiles, as confirmed by the low value of density changes within the reservoir (see Table S1 in the supporting information). Indeed, the reservoir lies at a depth where the most abundant gas phases at Mount Etna are already exsolved. As evidence, recharging phases have been accompanied with high gas flux emissions, preceding paroxysm activity and lava fountaining episodes, in which the gas-rich magma, supplied from the feeding system, propels the lava fountains. Based on all these considerations, we suppose that magma compressibility represents a plausible mechanism to explain the discrepancy between the erupted volume and the reservoir deflation volume observed during the 25–26 lava fountains, while refilling of the shallow reservoir occurs gradually and at a low rate over the whole lava fountaining cycle.

The exploitation of the spatiotemporal maps of magma-induced deformation and gravity changes during the whole cycle of lava fountain events could provide estimates on volumetric balance between accumulated and erupted volumes and may allow for tracking the different phases of magma transfer processes toward the surface and for placing important time constraints on the rates of magma accumulation, pressure buildup, and drainage. Since consistent correlations between eruption sequences and shallow reservoir inflation periods have been documented at several volcanoes [*Wadge et al*., 2006; *Foroozan et al*., 2011], future studies based on the joint analysis and modeling of deformation and gravity data may allow testing the hypothesis of a continuous balancing between refilling and drainage of magma regulated by an internal overpressure threshold, which triggers the eruptive events.

Acknowledgments
We are indebted to G. Ganci, R. Napoli, and A. Sicali for their help during the gravity surveys. We are also grateful to D. Pellegrino, M. Pulvirenti, and M. Rossi for enabling the acquisition of GPS raw data. We thank ASI that has provided the Cosmo-SkyMed SAR data within the framework of the MED-SUV Project (European Union's Seventh Program for research, technological development, and demonstration) under grant 308665. Thanks are due to P. Lundgren, an anonymous reviewer, and the Editor A. Newman for their useful suggestions that improved the paper. Data used in this study can be obtained contacting the corresponding author.

References

Battaglia, M., J. Gottsmann, D. Carbone, and J. Fernandez (2008), 4D volcano gravimetry, *Geophysics*, *73*(6), doi:10.1190/1.2977792.
Behncke, B., S. Branca, R. A. Corsaro, E. De Beni, L. Miraglia, and C. Proietti (2014), The 2011–2012 summit activity of Mount Etna: Birth, growth and products of the new SE crater, *J. Volcanol. Geotherm. Res.*, *270*, 10–21, doi:10.1016/j.jvolgeores.2013.11.012.
Berardino, P., G. Fornaro, R. Lanari, and E. Sansosti (2002), A new algorithm for surface deformation monitoring based on small baseline differential SAR interferograms, *IEEE Trans. Geosci. Remote Sens.*, *40*(11), 2373–2383, doi:10.1109/TGRS.2002.803792.

Bonaccorso, A., and S. Calvari (2013), Major effusive eruptions and recent lava fountains: Balance between expected and erupted magma volumes at Etna volcano, *Geophys. Res. Lett.*, *40*, 1–5, doi:10.1002/2013GL058291.

Bonaccorso, A., A. Cannata, R. A. Corsaro, G. Di Grazia, S. Gambino, F. Greco, L. Miraglia, and A. Pistorio (2011a), Multidisciplinary investigation on a lava fountain preceding a flank eruption: The 10 May 2008 Etna case, *Geochem. Geophys. Geosyst.*, *12*, Q07009, doi:10.1029/2010GC003480.

Bonaccorso, A., et al. (2011b), Dynamics of a lava fountain revealed by geophysical, geochemical and thermal satellite measurements: The case of the 10 April 2011 Mt Etna eruption, *Geophys. Res. Lett.*, *38*, L24307, doi:10.1029/2011GL049637.

Bonaccorso, A., G. Currenti, A. Linde, and S. Sacks (2013), New data from borehole strainmeters to infer lava fountain sources (Etna 2011–2012), *Geophys. Res. Lett.*, *40*, 3579–3584, doi:10.1002/grl.50692.

Calvari, S., G. G. Salerno, L. Spampinato, M. Gouhier, A. La Spina, E. Pecora, A. J. L. Harris, P. Labazuy, E. Biale, and E. Boschi (2011), An unloading foam model to constrain Etna's 11–13 January 2011 lava fountaining episode, *J. Geophys. Res.*, *116*, B11207, doi:10.1029/2011JB008407.

Cannata, A., G. Spedalieri, B. Behncke, F. Cannavò, G. Di Grazia, S. Gambino, S. Gresta, S. Gurrieri, M. Liuzzo, and M. Palano (2015), Pressurization and depressurization phases inside the plumbing system of Mount Etna volcano: Evidence from a multiparametric approach, *J. Geophys. Res. Solid Earth*, *120*, 5965–5982, doi:10.1002/2015JB012227.

Carbone, D., G. Currenti, and C. Del Negro (2007), Elastic model for the gravity and elevation changes before the 2001 eruption of Etna volcano, *Bull. Volcanol.*, *69*, 553–562, doi:10.1007/s00445-006-0090-5.

Casu, F., M. Manzo, and R. Lanari (2006), A quantitative assessment of the SBAS algorithm performance for surface deformation retrieval, *Remote Sens. Environ.*, *102*(3/4), 195–210, doi:10.1016/j.rse.2006.01.023.

Corsaro, R. A., V. Di Renzo, S. Distefano, L. Miraglia, and L. Civetta (2013), Relationship between petrologic processes in the plumbing system of Mt. Etna and the dynamics of the eastern flank from 1995 to 2005, *J. Volcanol. Geotherm. Res.*, *251*, 75–89, doi:10.1016/j.jvolgeores.2012.02.010.

Corsaro, R., and L. Miraglia (2013), Composizione dei vetri dei prodotti emessi dal Nuovo Cratere di Sud-Est durante l'attività stromboliana del 15 e 16 dicembre 2013. Rapp. UFVG del 18/12/2013, Catania, Italy. [Available at www.ct.ingv.it.]

Currenti, G. (2014), Numerical evidences enabling to reconcile gravity and height changes in volcanic areas, *Geophys. J. Int.*, *197*(1), 164–173, doi:10.1093/gji/ggt507.

Currenti, G., C. Del Negro, and G. Ganci (2007), Modelling of ground deformation and gravity fields using finite element method: an application to Etna volcano, *Geophys. J. Int.*, *169*, 775–786, doi:10.1111/j.1365-246X.2007.03380.x.

Currenti, G., C. Del Negro, and G. Ganci (2008), Finite element modeling of ground deformation and gravity field at Mt Etna, *Ann. Geophys.*, *51*(1), 105–119, doi:10.4401/ag-3037.

De Beni, E., and B. Behncke (2013), Misure GPS del campo lavico e del nuovo cono di scorie del Cratere di SE, Etna Aggiornamento del 28 ottobre 2013. Rapp. UFVG del 28/10/2013, Catania, Italy. [Available at www.ct.ingv.it.]

De Beni, E., B. Behncke, S. Branca, I. Nicolosi, R. Carluccio, F. D'Ajello Caracciolo, and M. Chiappini (2015), The continuing story of Etna's New Southeast Crater (2012–2014): Evolution and volume calculations based on field surveys and aerophotogrammetry, *J. Volcanol. Geotherm. Res.*, *303*, 175–186, doi:10.1016/j.jvolgeores.2015.07.021.

Foroozan, R., D. Elsworth, B. Voight, and G. S. Mattioli (2011), Magmatic-metering controls the stopping and restarting of eruptions, *Geophys. Res. Lett.*, *38*, L05306, doi:10.1029/2010GL046591.

Ganci, G., A. J. L. Harris, C. Del Negro, Y. Guehenneux, A. Cappello, P. Labazuy, S. Calvari, and M. Gouhier (2012), A year of lava fountaining at Etna: Volumes from SEVIRI, *Geophys. Res. Lett.*, *39*, L06305, doi:10.1029/2012GL051026.

González, P. J., and M. Palano (2014), Mt. Etna 2001 eruption: New insights into the magmatic feeding system and the mechanical response of the western flank from a detailed geodetic dataset, *J. Volcanol. Geotherm. Res.*, *274*, 108–121, doi:10.1016/j.jvolgeores.2014.02.001.

Greco, F., G. Currenti, G. D'Agostino, A. Germak, R. Napoli, A. Pistorio, and C. Del Negro (2012), Combining relative and absolute gravity measurements to enhance volcano monitoring, *Bull. Volcanol.*, doi:10.1007/s00445-012-0630-0.

Greco, F., E. Biolcati, A. Pistorio, G. D'Agostino, A. Germak, C. Origlia, and C. Del Negro (2015), Absolute gravity measurements at three sites characterized by different environmental conditions using two portable ballistic gravimeters, *Eur. Phys. J. Plus*, *130*, 38–47, doi:10.1140/epjp/i2015-15038-0.

Herring, T. A., R. W. King, and S. C. McClusky (2010), *Introduction to GAMIT/GLOBK, Release 10.4*, pp. 1–48 Massachusetts Institute of Technology, Cambridge, Mass.

Kozono, T., H. Ueda, T. Ozawa, T. Koyaguchi, E. Fujita, A. Tomiya, and Y. J. Suzuki (2013), Magma discharge variations during the 2011 eruptions of Shinmoe-dake volcano, Japan, revealed by geodetic and satellite observations, *Bull. Volcanol.*, *75*, 695, doi:10.1007/s00445-013-0695-4.

Maucourant, S., S. Giammanco, F. Greco, S. Dorizon, and C. Del Negro (2014), Geophysical and geochemical methods applied to investigate fissure-related hydrothermal systems on the summit area of Mt. Etna volcano (Italy), *J. Volcanol. Geotherm. Res.*, *280*, 111–125, doi:10.1016/j.jvolgeores.2014.05.014.

Palano, M., E. Guarrera, and M. Mattia (2012), GPS ground deformation patterns at Mount St. Helens (Washington, USA) from 2004 to 2010, *Terra Nova*, *24*, 148–155, doi:10.1111/j.1365-3121.2011.01049.x.

Patanè, D., et al. (2013), Insights into magma and fluid transfer at Mount Etna by a multiparametric approach: A model of the events leading to the 2011 eruptive cycle, *J. Geophys. Res. Solid Earth*, *118*, 3519–3539, doi:10.1002/jgrb.50248.

Pepe, A., and R. Lanari (2006), On the extension of the minimum cost flow algorithm for phase unwrapping of multitemporal differential SAR interferograms, *IEEE Trans. Geosci Remote Sens.*, *44*(9), 2374–2383, doi:10.1109/TGRS.2006.873207.

Pistorio, A., F. Greco, G. Currenti, R. Napoli, A. Sicali, C. Del Negro, and L. Fortuna (2011), High-precision gravity measurements using absolute and relative gravimeters at Mount Etna (Sicily, Italy), *Ann. Geophys.*, *54*(5), 500–509, doi:10.4401/ag-5348.

Trasatti, E., and M. Bonafede (2008), Gravity changes due to overpressure sources in 3D heterogeneous media: Application to Campi Flegrei caldera, Italy, *Ann. Geophys.*, *51*(1), 119–133, doi:10.4401/ag-4442.

Wadge, G., D. Oramas Dorta, and P. D. Cole (2006), The magma budget of Volcán Arenal, Costa Rica from 1980 to 2004, *J. Volcanol. Geotherm. Res.*, *157*, 60–74, doi:10.1016/j.jvolgeores.2006.03.037.

Yang, Y., A. Pepe, M. Manzo, F. Casu, and R. Lanari (2013), A region-growing technique to improve multi-temporal DInSAR interferogram phase unwrapping performance, *Remote Sens. Lett.*, *4*, 988–997, doi:10.1080/2150704X.2013.826835.